Thierry Lefèvre
Karin Arseneault
Michel Pézolet
Centre de Recherche en Sciences et Ingénierie des Macromolécules, Département de Chimie, Université Laval, Québec (Québec) G1K 7P4, Canada

Study of Protein Aggregation Using Two-Dimensional Correlation Infrared Spectroscopy and Spectral Simulations

Received 2 September 2003; accepted 3 November 2003
Published online 8 March 2004 in Wiley InterScience (www.interscience.wiley.com). DOI 10.1002/bip.20010

Abstract: *Two-dimensional (2D) correlation spectroscopy establishes correlations between intensity variations in a series of spectra obtained by the application of an external perturbation. However, spectral effects (wavenumber shift or bandwidth change) are known to generate apparent asynchronisms in 2D maps. Surprisingly, spectral effects are often neglected in the literature when interpreting experimental maps, which can lead to erroneous conclusions. In an attempt to evaluate the contribution of these effects and that of true asynchronisms on 2D maps, the heat-induced aggregation of glutamyl-tRNA synthetase (GluRS) was studied as a typical example of the application of Fourier transform infrared (FTIR) spectroscopy in the amide I region. The data were compared with those obtained from a mutant protein that differs by one amino acid. To determine whether the aggregation mechanisms are identical for both proteins, the experimental 2D maps were compared to simulations based on curve fitting of the initial and final spectra of the series, which allows change in position and bandwidth of the components to be taken into account. Intermediate spectra were generated using a convenient function that mimics the spectral evolution. The speed and the delay of each component were controlled. Apart from the appearance of turns that occur for the mutant and not for GluRS, the aggregation mechanisms of both proteins seems to be essentially identical. In particular, the loss of α-helices seems to be concomitant with the formation of intermolecular β-sheets, whereas the loss of intramolecular β-sheets is delayed. Since the experimental maps are satisfactorily simulated when almost all the components are in phase, it appears that many of the asynchronous features are mainly due to spectral effects. Thus, one has to be aware that* true *asynchronisms are not necessarily at the origin of peaks observed in asynchronous maps.* © 2004 Wiley Periodicals, Inc. Biopolymers 73: 705–715, 2004

Keywords: *two-dimensional infrared correlation spectroscopy; Fourier transform infrared spectroscopy; protein; heat-induced aggregation; glutamyl–tRNA synthetase*

Correspondence to: Michel Pézolet; email: michel.pezolet@chm.ulaval.ca

Contract grant sponsor: Natural Science and Engineering Research Council (NSERC) of Canada, Fonds Québécois de la Recherche sur la Nature et les Technologies (FQRNT), and Centre de Recherche en Sciences et Ingénierie des Macromolécules (CERSIM)

INTRODUCTION

Infrared spectroscopy is a very versatile and useful technique for the characterization of many aspects of protein structure.[1–3] For example, this technique has been used to probe protein conformation and stability under different aqueous environments and to characterize structural changes that occur during denaturation such as unfolding and aggregation. The amide I mode of the peptide bond is the most studied vibration since it is particularly sensitive to the type of secondary structure.[4] This band consists of the complex overlapping of components due to the different secondary structure elements that compose the protein architecture. As a consequence, the amide I band is broad and ill-defined, and it is often difficult to analyze. The so-called resolution enhancement tools such as Fourier deconvolution[1,5,6] allow to distinguish the components present under broad absorption bands, to discriminate between secondary structures, and to detect subtle conformational modifications.

More recently, Noda has developed a spectral analysis method called two-dimensional correlation spectroscopy (2D-COS).[7–9] The aim of this mathematical tool is to emphasize in-phase and out-of-phase correlations between spectral intensity variations occurring at different wavenumbers that are induced by the application of an external perturbation on the studied system. This method offers several potential advantages. First, it may simplify complex spectra like a resolution enhancement technique. For example, two overlapping and indistinguishable bands with different dynamic response may theoretically be separated. In addition, it may allow the establishment of band assignments. Indeed, by studying correlations between bands located in different spectral regions, it is possible, if their intensity variations are synchronously correlated, to assign them to the vibration of the same structural element. Finally, this technique can be useful to identify asynchronisms in a series of spectra. It is then potentially possible to establish a sequence of events during a physical or chemical process.

Thus, 2D-COS seems to be especially suited for proteins since they give rise to broad bands and undergo complex (multistep) phenomena when an external perturbation is applied. Among many applications to proteins, 2D-COS has allowed the investigation of correlations between amide I, amide II, or amide III bands,[10,11] or between bands in the mid- and near-ir regions.[12–14] It has also been applied to the analysis of the kinetics of the hydrogen/deuterium exchange of the amide groups in order to obtain information relative to the flexibility and solvent accessibility of the protein secondary structures.[10,11] Finally, it has extensively been used to get insights into the sequence of events occurring during protein denaturation induced by temperature,[15–18] pressure,[19] or pH.[20]

Most studies using 2D-COS have interpreted the asynchronous maps in terms of hierarchical orders of events. However, it has been demonstrated that other effects than true asynchronisms, such as wavenumber shifts and bandwidth changes (called spectral effects hereafter), can generate apparent asynchronous peaks. This has specifically been shown with model simulations.[21–23] For example, a single band that shifts or broadens with the perturbation gives asynchronous peaks with itself. It also creates asynchronous peaks with another band even if the intensity changes of the latter are totally synchronous with the first one and even if this second band is not subjected to spectral effects. Surprisingly, the spectral effects are often neglected when interpreting experimental maps. This can lead to erroneous conclusions, especially for highly overlapping bands. Indeed, 2D peaks may be attributed to true asynchronisms when they actually originate from bandwidth change or wavenumber shift (apparent asynchronisms). The detection of spectral effects is important since they represent physical changes that have to be taken into account to understand the molecular modifications occurring during the application of an external perturbation. For example, a shift of the amide I components could indicate a modification of the local environment of the peptide bond or a change in the hydrogen bond strength, whereas a band broadening can reflect a change in the flexibility or mobility of the secondary structure elements.

The aim of the present work is to evaluate the contribution of spectral effects on experimental 2D maps in a highly overlapping spectral region. As a typical example, we have analyzed the effect of temperature on the amide I band of glutamyl–tRNA synthetase (GluRS) from *Escherichia coli*. The enzymes of the synthetase family catalyze the aminoacylation of transfer RNA (tRNA).[24,25] Since this reaction consists of the binding of the correct amino acid to the correct tRNA, the synthetases are involved in the transfer of the genetic information. GluRS contains 471 amino acids and its molecular weight is of about 54,000 Da.[26] Its secondary structure mainly consists of α-helices with a few β-sheets and -turns. GluRS contains a glycine at position 254 (Gly^{254}) that is universally conserved. It is has been proposed that this amino acid can have a crucial functional and/or structural role. To determine the importance of this amino acid, we have compared the thermal stability of

GluRS with that of a mutant protein ($G_{254}R$) obtained by the replacement of the Gly^{254} by an arginine. We thus took advantage of using 2D-COS to get insight into the aggregation mechanism of both proteins.

MATERIALS AND METHODS

Materials and Sample Preparation

GluRS and $G_{254}R$ were purified from *E. coli* as described elsewhere.[27] The proteins were lyophilized and then dissolved in 20 m*M* HEPES–KOH [HEPES: *N*-(2hydroxythyl)piperazine-*N*′-ethanesulfonic acid] buffer in D_2O (CDN Isotopes, Sainte-Claire, PQ, Canada) at pD 7.6 and a concentration of 20 mg/mL.

IR Spectroscopy

A volume of 27 μL of the protein solution was deposited between the two CaF_2 windows of a Biocell™ from Biotools, Inc. (Elmhurst, IL), manufactured with a calibrated pathlength of 50 μm. The transmission spectra were recorded at a resolution of 2 or 4 cm^{-1} with a Nicolet Magna 850 spectrometer (Thermo-Nicolet, Madison, WI) equipped with a narrow band MCT detector and continuously purged with dry air. For each spectrum, 200 scans were coadded and apodized with a Happ–Genzel function. The temperature was computer controlled with a Omega temperature controller (Stamford, CT). The samples were heated between 25 and 69°C with steps of 2°C and were equilibrated for 5 min at the desired temperature before recording the spectra.

The whole treatment of the amide I band (the so-called amide I′ band for deuterated peptide groups) was made with the Grams/32 software version 5.1 (Galactic Industries Corp., Salem, NH). For each temperature, the spectrum of the buffer solution at the appropriate temperature was subtracted from that of the protein solution (subtraction factor of 1 for all temperatures). Water vapor was subtracted, the subtraction factor being optimized using the autosubtract function. For the study of the amide I′ region, a linear baseline correction was performed between 1700 and 1595 cm^{-1}. To avoid nondesirable intensity variations, all the spectra were normalized to give an area of 1 in this spectral range. The dynamic spectra were calculated by subtracting to each normalized spectrum of a given series the first normalized spectrum recorded (subtraction factor of 1). A series corresponds to the heating of a sample from the onset to the end of aggregation. The onset of aggregation was assessed from the temperature at which the intensity at 1618 cm^{-1} starts to increase, and the end was determined by the temperature at which the intensity at 1618 cm^{-1} remains constant.

Two-Dimensional Correlation Analysis

The synchronous (Φ) and asynchronous (Φ) matrixes were calculated and the corresponding maps plotted with a program written with Mathlab 5.3 for Windows (MathSoft Inc., Cambridge, MA). The calculation was carried out in the matrix form[28] using the Hilbert transform[29]:

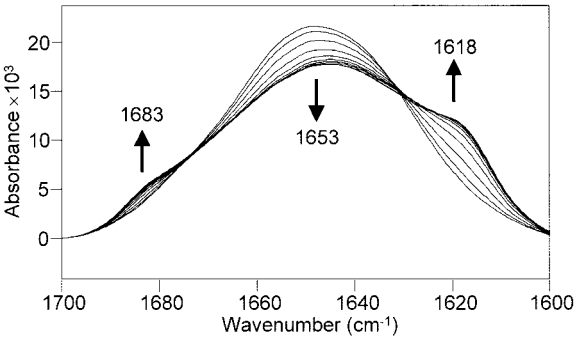

FIGURE 1 Normalized spectra of GluRS in D_2O buffer in the amide I′ region recorded between 47 and 67°C. The arrows indicate the intensity variations as the temperature increases.

$$\Phi = \frac{1}{n-1} M M^T$$

and

$$\psi = \frac{1}{n-1} M(HM^T)$$

where n is the number of the spectra in the series, M is the matrix of spectra (spectra are put in columns), M^T is the transposed matrix of M, and H is the Hilbert–Noda transform matrix whose elements $H_{mn} = 0$ if $m = n$, and $H_{mn} = 1/\pi\ (n-m)$ otherwise.[29]

A filter was used to eliminate weak intensities. It sets to zero the elements Φ_{mn} of Φ and Ψ_{mn} of Ψ that obey the conditions:

$$|\Phi_{mn}| < (\Phi_{max} - \Phi_{min})/100$$

and

$$|\psi_{mn}| < (\psi_{max} - \psi_{min})/100$$

respectively.

RESULTS AND DISCUSSION

Experimental Spectra and 2D Maps of GluRS

Figure 1 shows the normalized spectra of GluRS in aqueous solution as a function of temperature from 47 to 67°C in the amide I′ region. As the temperature increases, two shoulders near 1683 and 1618 cm^{-1} appear, as it has often been observed for proteins

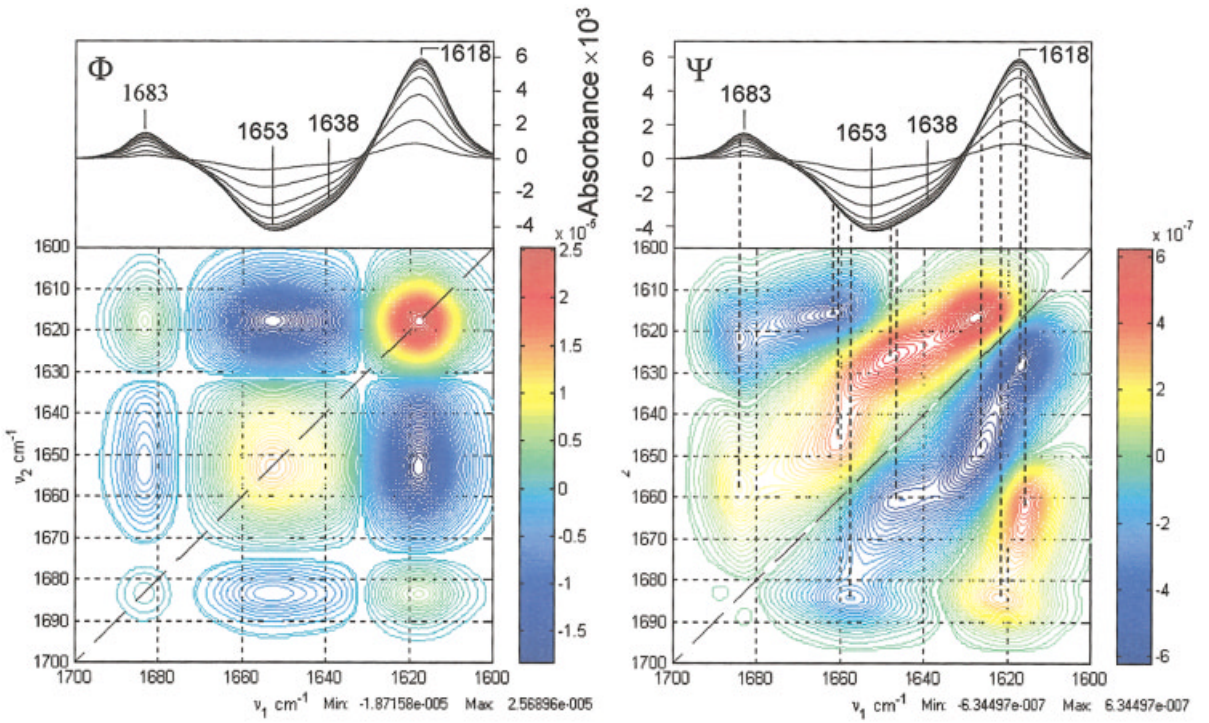

FIGURE 2 Synchronous and asynchronous maps Φ and Ψ generated by the spectra of Figure 1.

undergoing self-aggregation.[17,30–33] The component at 1618 cm^{-1} is assigned to intermolecular β-sheets[34,35] and the component at 1683 cm^{-1} reveals that they are antiparallel.[4] The formation of these intermolecular hydrogen bonds is accompanied by an intensity decrease of a broad band centered near 1653 cm^{-1} assigned to the loss of native secondary structures.

Figure 2 shows the synchronous (Φ) and asynchronous (Ψ) maps generated from the spectra of Figure 1. The dynamic spectra used for the calculation are represented in the outer frames. They clearly reveal the intensity increase at 1683 and 1618 cm^{-1}, and the intensity decrease of the broad band at 1653 cm^{-1}. A shoulder near 1638 cm^{-1} indicates that this broad feature is actually composed of two components assigned to α-helices (1653 cm^{-1}) and intramolecular β-sheets (1638 cm^{-1}). The synchronous map shows a strong autopeak at 1618 cm^{-1}, a broad less intense one at 1653 cm^{-1}, and a weak one at 1683 cm^{-1}. These peaks represent the intensities that evolve as a result of the application of the perturbation. The signs of the cross peaks indicate that the intensity near 1653 cm^{-1} varies in the opposite direction than the intensity at 1618 and 1683 cm^{-1}. Essentially, the synchronous map gives the same information than the one-dimensional (1D) spectra.

The asynchronous map shows two elongated features nearly parallel to the diagonal with different peak maxima, in particular a strong one at 1616/1625 cm^{-1} and a weaker one at 1626/1647 cm^{-1}. It also reveals two elongated satellite features with maxima at 1615/1662 and 1621/1684 cm^{-1}. The interpretation of this map is not straightforward. How can one interpret such features and what is their origin? As mentioned above, the spectra of GluRS can be decomposed in four components, and there is a priori no justified reason to assess the existence of other components. Nevertheless, the asynchronous map contains peaks located near 1627, 1647, and 1662 cm^{-1} that do not have to be assigned to "new" components whose intensity variations are delayed (or advanced) or would have a different evolution speed. The vertical dotted lines on Figure 2 clearly shows that the positions of some 2D peak maxima do not correspond to the position of the components of GluRS.

In general, the position, intensity, and shape of the 2D asynchronous peaks are influenced by many factors including the presence of asynchronism (out-of-phase intensity variation), the type of spectral effect (band shift and broadening or narrowing), the amplitude of the spectral variations,[21,22] and the shape of the band (for example, it can be demonstrated that the 2D maps obtained from Lorentzian and Gaussian bands are different). Thus, the 2D peaks contain the information relative to a mixture of different spectral changes. In a attempt to determine the spectral

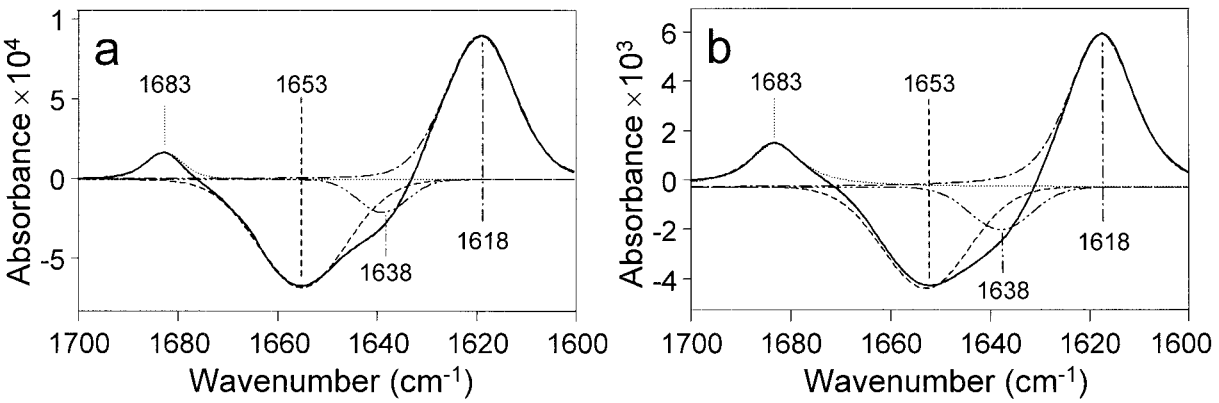

FIGURE 3 (a) Initial dynamic spectrum of GluRS at 49°C and (b) final one at 67°C curve fitted with four components. The simulated and experimental spectra are almost indistinguishable.

changes that generate the 2D maps of Figure 2, the following spectral simulation has been performed.

The Method Used to Generate Simulated Spectra

1. In a first step, the experimental dynamic spectra are calculated by subtraction of the first spectrum of the series recorded at the onset of aggregation. Spectral decomposition (curve fitting) is then carried out on the initial and final dynamic spectra. A similar approach was adopted by Schultz et al.,[15] who modeled the denaturation process with four bands, two decreasing ones representing the unfolding and two increasing ones representing the aggregation. They use the original spectra for curve fitting. We have preferred to fit dynamic spectra because this dramatically restricts the number of possible fits with respect to the large number of solutions that could be found when using the original spectra. Attention has been paid to decompose the spectra with the minimum number of components. Only significant components, as deduced from the difference and/or second derivative spectra, are taken into account. The components are modeled with Gaussian/Lorentzian functions with a Lorentzian proportion denoted as lg. The first dynamic spectrum of the series is actually zero since it results from the subtraction of the first original spectrum by itself. Thus, to be able to make the curve fitting, the initial spectrum was in fact the second dynamic spectrum of the series. The 2D maps generated by the original spectra using the first spectrum as reference was very close to the 2D maps generated by the dynamic spectra with no reference when the first (null) difference spectrum was neglected. Figure 3 shows the dynamic spectra of the initial and final spectrum of the series of Figure 1 and the typical fits obtained. For GluRS, four components located at 1618, 1638, 1653, and 1683 cm^{-1} were used. These fits provide, for each component, the initial and final values of the wavenumber ν_j, the width at half-height $\Delta\nu_j$, the intensity I_j, and the Lorentzian proportion lg_j. The subscript j labels each component, so j varies between 1 and N, where N is the total number of components that are necessary to make the fit. For simplicity, we assume that the increase in temperature only results in change in intensity, wavenumber, and bandwidth, and that each band keeps the same shape during the experiment. Thus lg_j is kept constant for the all simulated spectra of the series and is arbitrary chosen to be equal to the final value obtained.

2. The second step consists in the generation of the intermediate simulated spectra that reflect the spectral variations from the initial to the final experimental spectrum. To join the initial and the final values of the band parameters, the hyperbolic tangent function was chosen:

$$\mathrm{th}(\alpha_j(t+\beta_j)) = \frac{\exp(\alpha_j(t+\beta_j)) - \exp(-\alpha_j(t+\beta_j))}{\exp(\alpha_j(t+\beta_j)) + \exp(-\alpha_j(t+\beta_j))}$$

where α_j is the slope of the curve for $t = -\beta_j$ (it represents the "speed" of the parameter variation), β_j represents a potential delay (β_j is negative for a delay and positive when the parameter's variation is in advance), and t is the variable that describes the external perturbation. Other functions could be used, but this function is a good representation of phenomena such as phase transitions, titration curves, etc.

Figure 4 illustrates a plot of the typical evolution of a parameter as a function of t. Examples of delayed or faster variations are also shown. Let us call $p_j(\alpha_j,\beta_j,t)$ a parameter of the jth component [characterizing the wavenumber $\nu_j(\alpha_j,\beta_j,t)$, width at half-height $\Delta\nu$

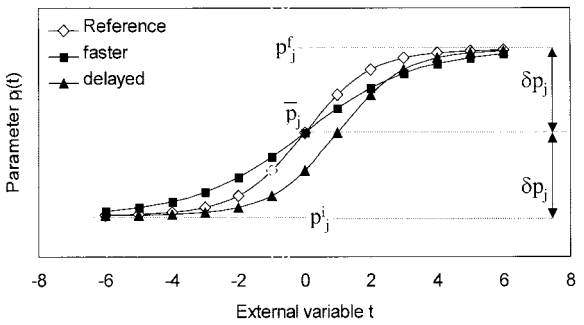

FIGURE 4 Plot of the variation of the parameter $p_j(t)$ using a hyperbolic tangent function between its initial (p^i_j) and final (p^f_j) values. Full squares: reference with $\alpha = 0.5$ and $\beta = 0$; empty circles: the same with a smaller value of α (α =0.3); full triangles: delayed variation of $p_j(t)$ when $\beta = -1$. The mean value $\bar{p}_j(t)$ and the half-amplitude δp_j of the spectral variation are also indicated.

$_j(\alpha_j,\beta_j,t)$, or intensity $I_j(\alpha_j,\beta_j,t)$] that evolves from its initial value p^i_j to its final value p^f_j as a function of the external variable t. It can be written as

$$p_j(\alpha_j,\beta_j,t) = \bar{p}_j + \delta p_j \mathrm{th}(\alpha_j(t+\beta_j)),$$

with

$$\bar{p}_j = \frac{p_j^i + p_j^f}{2}$$

$$\delta p_j = \frac{p_j^f - p_j^i}{2}$$

$\bar{p}_j$ and δp_j correspond to the mean value and half-amplitude of the variation of $p_j(\alpha_j,\beta_j,t)$, respectively.

The variable t was chosen to vary between -6 and $+6$ by steps of unity since $p_j(\alpha_j,\beta_j,t=-6) \approx p^i_j$ and $p_j(\alpha_j,\beta_j,t=6) \approx p^f_j$ [for example, for $\alpha_j = 0.5$ and $\beta_j = 0$, which are typical values used in this work, $\mathrm{th}(0.5\times6) = -\mathrm{th}(0.5\times-6) = 0.995$]. Hence, the values of the delay have to be compared with the total range of variation of t, which is 12 units. Thirteen dynamic spectra $\tilde{y}(\alpha_j,\beta_j,\nu,t)$ (eleven intermediate ones in the simulated series) are then generated using the following formula:

$$\tilde{y}(\alpha_j,\beta_j,\nu,t) = \sum_{j=1}^{N} \left\{ lg \cdot \frac{I_j(\alpha_j,\beta_j,t)}{1 + \left(\dfrac{\nu - \nu_j(\alpha_j,\beta_j,t)}{\Delta\nu_j(\alpha_j,\beta_j,t)/2} \right)^2} + (1 - lg) \cdot I_j(\alpha_j,\beta_j,t) \cdot \exp\left[-\ln 2 \left(\frac{\nu - \nu_j(\alpha_j,\beta_j,t)}{\Delta\nu_j(\alpha_j,\beta_j,t)/2} \right)^2 \right] \right\}$$

It is assumed that, in any case, the three parameters $\nu_j(\alpha_j,\beta_j,t)$, $\Delta\mu_j(\alpha_j,\beta_j,t)$, and $I_j(\alpha_j,\beta_j,t)$ of the j^{t}h component vary totally in-phase (same α_j and same β_j for a given j), but the speed and delays can be different for each component.

3. For the reasons given above, the simulated maps are calculated with no reference using the initial dynamic spectrum (second spectra of the series) and the final one (last one). It is first assumed that all the components vary in phase. The corresponding simulated maps are then compared to the experimental ones, and if differences too large are observed, some components are delayed or advanced. We observed that in general the synchronous maps are relatively easy to simulate, i.e., to reproduce the position, size, and shape of the 2D peaks. This is because the 2D peak shape is not strongly affected by the asynchronisms between the components and by the spectral effects. They are rather strongly influenced by the shape of the bands (i.e., by lg), by the amplitude, and by the direction of the intensity changes. The experimental asynchronous maps are more difficult to simulate because they are highly characteristic of all the spectral variations. As a spectrum is considered as a fingerprint of a compound, an asynchronous map can be considered as a fingerprint of the spectral variations in a series of spectra.

Application of the Method: Comparison Between GluRS and $G_{254}R$

Figure 5 shows the Φ and Ψ 2D maps and the simulated dynamic spectra corresponding to the experimental data of Figure 1. They were obtained when all components vary synchronously (α= 0.5 and β = 0 for all) except the component at 1638 cm^{-1}, which is delayed by 0.5 unit of the external parameter. The simulated maps are very similar to the experimental ones in terms of shape, size, position, and number of the peaks. Small differences are found in some peak shapes and peak intensities, but the overall pattern and many details are well reproduced. In addition, all of the peak maxima are located at identical positions. Therefore, the results can be considered as satisfactory, especially if one considers the complexity of the experimental maps. To improve the simulated results, we have tried to change the value of α and β for some components, but any modification led to maps that were not as good as those of Figure 5. Therefore, it can be assessed that the heat-induced aggregation of GluRS results from the formation of intermolecular antiparallel β-sheets (components at 1618 and 1683 cm^{-1}) that is basically concomitant to the loss of helical structures, while the loss of intramolecular β-sheets is delayed.

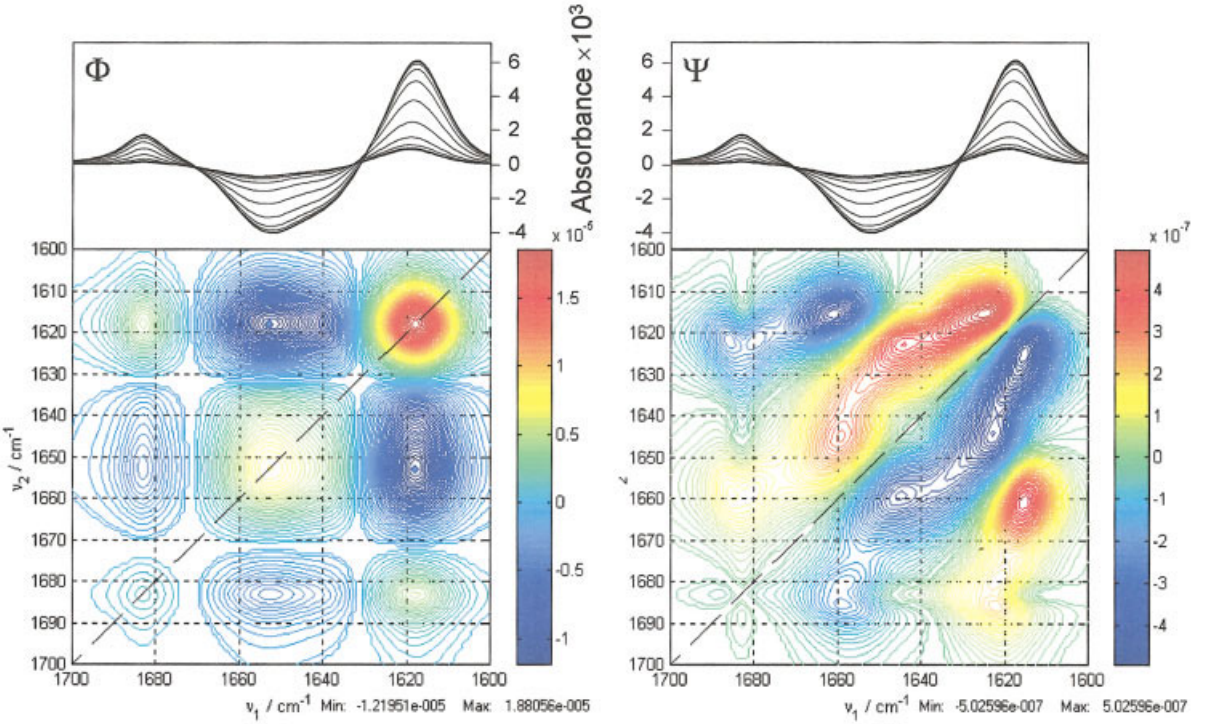

FIGURE 5 Simulated synchronous and asynchronous maps corresponding to Figure 2. The simulated spectra are made up with 4 components located at 1683, 1653, 1638, and 1618 cm^{-1}. The spectral variations of the different components were made with $\alpha = 0.5$ for all. The values of β is 0 for all, except the component at 1638 cm^{-1} for which $\beta = -0.5$.

Figure 5 is a typical and interesting example showing that the superposition of component variations with only one delayed component can lead to a complex asynchronous map. If all the components vary totally in phase, the asynchronous map is as complex as that of Figure 5 (maps not shown) but does not reproduce as well the experimental maps. Thus, it is clear that many of the 2D asynchronous peaks only originate from wavenumber shifts and bandwidth changes. This can also be seen in Table I, where the different band parameters resulting from band fitting are shown: each component undergoes a wavenumber shift and band broadening or narrowing.

An advantage of this simulation method lies in the control of each component parameter and in the estimation of the impact of spectral effects on the 2D maps by keeping ν and/or $\Delta\nu$ constant for the spectra of the series. An example is given in Figure 6a, where the simulated asynchronous map of Figure 5 is shown when the position of the 1618−cm^{-1} component is kept constant. Many modifications can be observed, especially the shift to lower wavenumbers of the strong 2D peak initially located at 1616/1625 cm^{-1} (labeled with a pink dot). The peak intensities at 1660/1647 and 1615/1662 cm^{-1} also significantly

Table I Results of the Band Fitting of the Initial and Final Spectra of the Series Corresponding to the Heat-Induced Aggregation of GluRS[a]

	Initial Spectrum	Final Spectrum
Component 1	$\nu_1^i = 1683.0\ cm^{-1}$ $I_1^i = 1.7\ 10^{-4}$ $\Delta\nu_1^i = 8.8\ cm^{-1}$	$\nu_1^f = 1683.1\ cm^{-1}$ $I_1^f = 1.7\ 10^{-3}$ $\Delta\nu_1^f = 12.6\ cm^{-1}$
Component 2	$\nu_2^i = 1655.2\ cm^{-1}$ $I_2^i = -6.8\ 10^{-4}$ $\Delta\nu_2^i = 21.0\ cm^{-1}$	$\nu_2^f = 1653.0\ cm^{-1}$ $I_2^f = -4.1\ 10^{-3}$ $\Delta\nu_2^f = 20.5\ cm^{-1}$
Component 3	$\nu_3^i = 1638.9\ cm^{-1}$ $I_3^i = -2.1\ 10^{-4}$ $\Delta\nu_3^i = 11.7\ cm^{-1}$	$\nu_3^f = 1637.9\ cm^{-1}$ $I_3^f = -1.7\ 10^{-3}$ $\Delta\nu_3^f = 14.4\ cm^{-1}$
Component 4	$\nu_4^i = 1619.3\ cm^{-1}$ $I_4^i = 9.0\ 10^{-4}$ $\Delta\nu_4^i = 16.6\ cm^{-1}$	$\nu_4^f = 1617.7\ cm^{-1}$ $I_4^f = 6.2\ 10^{-3}$ $\Delta\nu_4^f = 15.8\ cm^{-1}$

[a]The values of the different parameters (wavenumber, intensity, and width at half height) are given for each component.

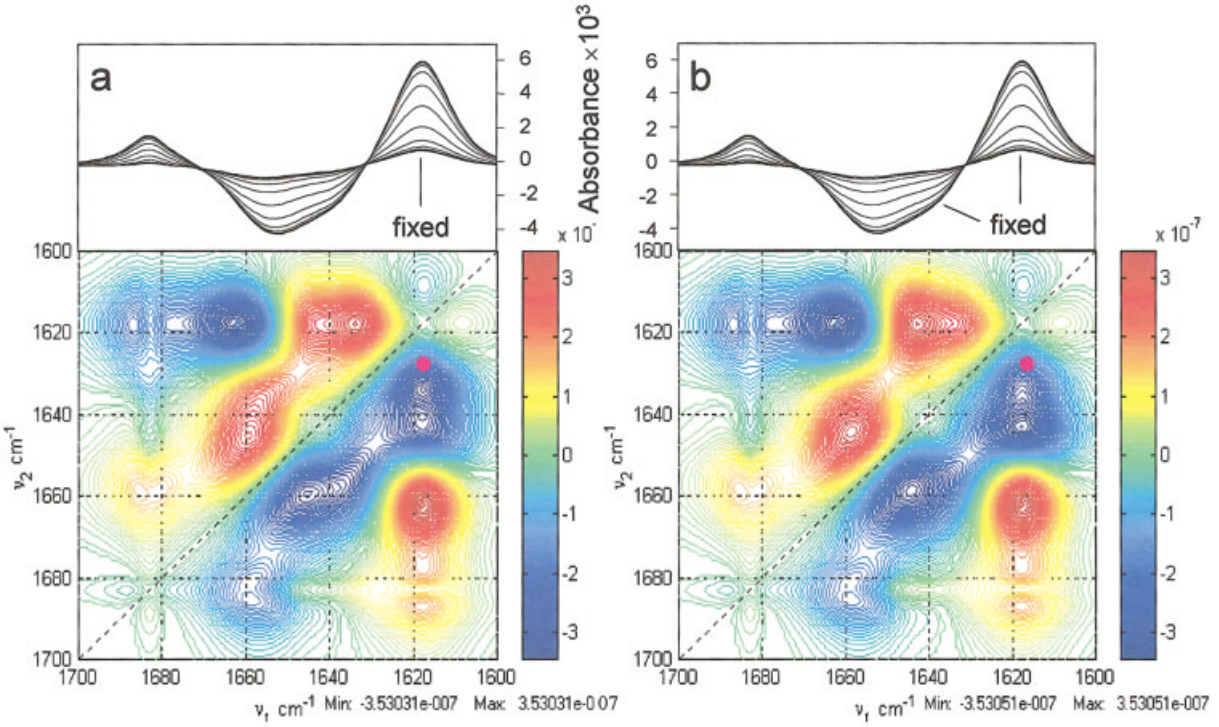

FIGURE 6 The same spectral simulations as in FIGURE 5 when (a) the position of the 1638-cm^{-1} component is kept constant and (b) when the position of both components at 1618 and 1638 cm^{-1} are kept constant. The pink point indicates the position of the 2D peak initially located at 1616/1625 cm^{-1} in Figure 5.

increases. This example shows that the shift of the band at 1618 cm^{-1} is determinant for the presence of the peak at 1616/1625 cm^{-1} and it exemplifies the significant impact of a simple wavenumber shift can have on the general pattern of Ψ. If now the position of the 1638-cm^{-1} component is also kept constant (Figure 6b), the peak maxima at 1616/1625 cm^{-1} in Figure 5 is replaced by another one at 1618/1643 cm^{-1}. No additional modifications are observed for the 2D peaks located below 1650 cm^{-1}. In conclusion, these observations show that the evolution of a band can create 2D peaks by itself, but they can also be strongly influenced by other components without any true asynchronism between the intensity variations.

Figure 7 shows a comparison of the normalized spectra of GluRS and $G_{254}R$ at the onset and at the end of the aggregation as well as the dynamic spectra corresponding to the heat-induced aggregation of both proteins. For $G_{254}R$, the spectra are recorded from 45 to 69°C. The spectra at the onset of aggregation (Figure 7a) exhibit strong differences due to the fact that in their native states $G_{254}R$ may be in a higher oligomeric form than the wild-type protein.[27] On the contrary, the spectra are identical at the end of aggregation (Figure 7b), indicating identical structures in the aggregated state. Since the initial spectra are different while the final ones are identical, the spectral variations of the dynamic spectra must be different. Indeed, a weak component near 1670 cm^{-1}, assigned to turn structures, appears for $G_{254}R$ but is absent for GluRS (Figure 7c and 7d). This component was absolutely required to achieve good spectral fits of the dynamic spectra of $G_{254}R$. Another difference is the position of the band assigned to native structures, which is located at 1649 cm^{-1} for $G_{254}R$ and 1653 cm^{-1} for GluRS. Since the spectral variations of the dynamic spectra are different for both proteins, it can be anticipated that their 2D maps will be different.

The experimental synchronous map generated by the dynamic spectra of $G_{254}R$ is almost identical to that of GluRS (not shown). It reflects the formation of intermolecular β-sheets at the expense of native structures like for GluRS. A small difference in the position of the broad autopeak in the middle of the map (1653 cm^{-1} for GluRS and 1649 cm^{-1} for $G_{254}R$) reflects the difference in the position of the broad band due to the loss of native structures as discussed above. In addition, the broadening of the 2D peaks at 1683 cm^{-1} towards lower wavenumber for $G_{254}R$

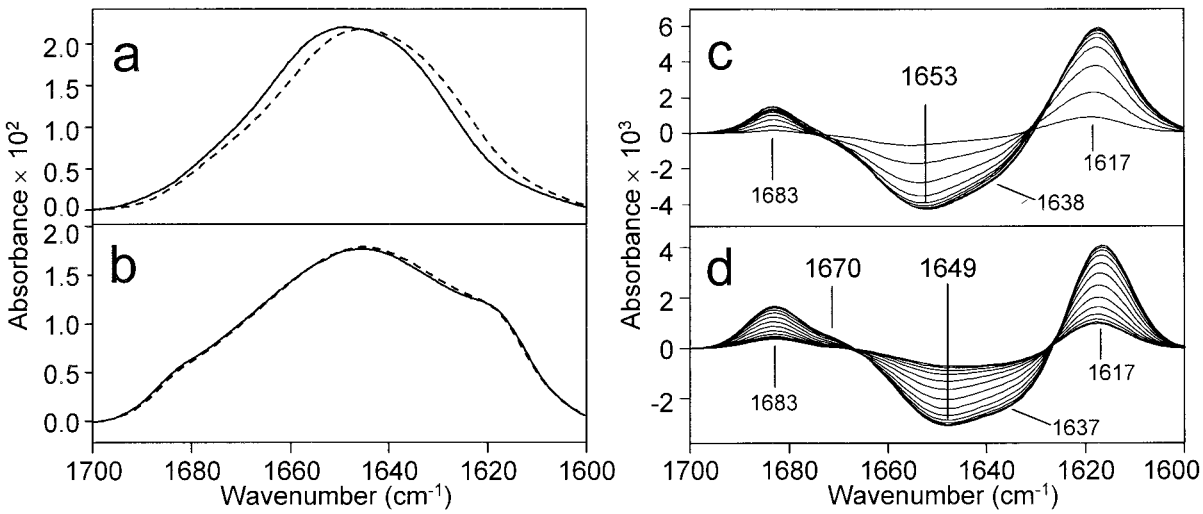

FIGURE 7 Normalized spectra of GluRS (full lines) and $G_{254}R$ (dotted lines) (a) at the onset (initial spectra) and (b) at the end (final spectra) of aggregation. Dynamic spectra corresponding to the heat-induced aggregation of (c) GluRS and (d) $G_{254}R$.

(absent for the GluRS) reflects the presence of the component at 1670 cm^{-1}. Figure 8a shows the asynchronous map generated by the dynamic spectra of $G_{254}R$ shown in Figure 7d. It shares common points with those of GluRS (Figure 2). Both maps have a similar pattern including the elongated features along

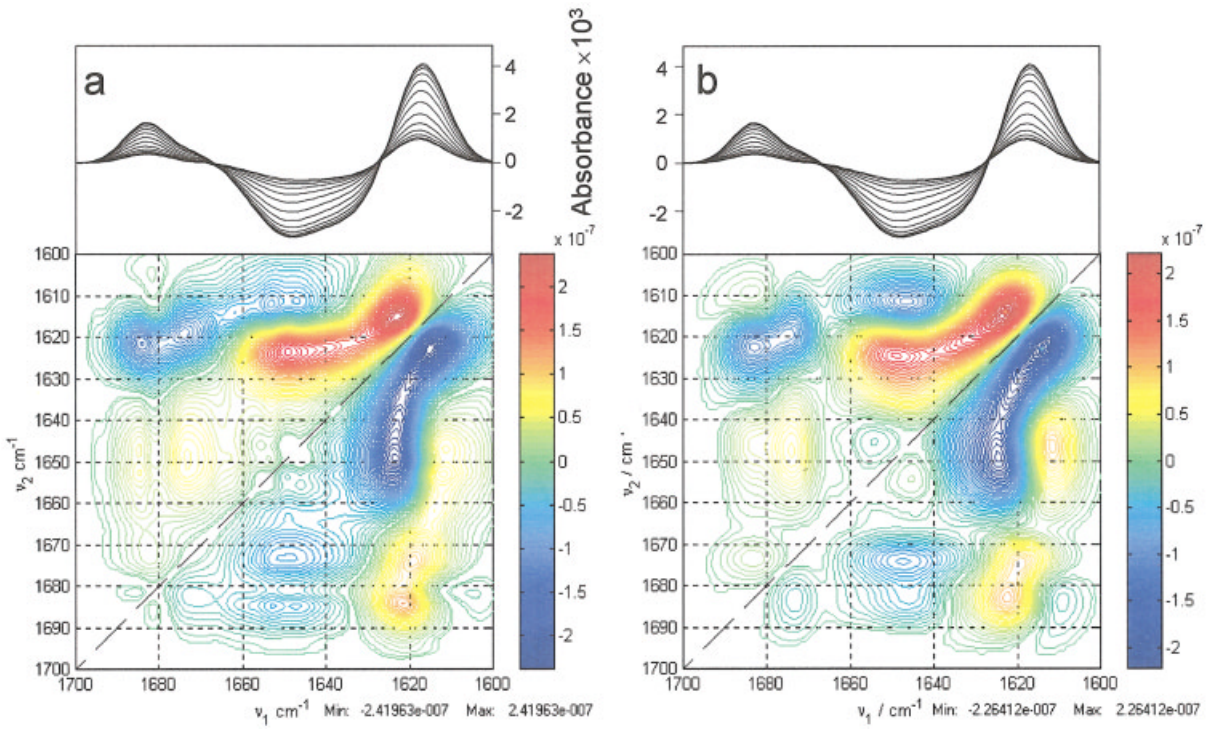

FIGURE 8 (a) Experimental asynchronous map generated by the experimental spectra of $G_{254}R$ and (b) corresponding simulated asynchronous map. The simulated spectra are made up with 5 components located at 1683, 1670, 1651, 1637, and 1618 cm^{-1}. The spectral variations of the different components are made with $\alpha = 0.5$ for all. The values of β is 0 for all, except the component at 1670 and 1638 cm^{-1} for which $\beta = -0.5$.

the diagonal and the satellite ones. Many peak maxima are located at very close wavenumber values for the wild-type and the mutant proteins, but obvious differences are also observed. However, are they only related to the above differences in the spectral variations or are there additional effects due to different hierarchical orders of the intensity variations? In other words, is there differences in the aggregation mechanisms of both proteins?

To answer this question we have performed spectral simulations. Figure 8b shows the asynchronous map generated by simulated spectra corresponding to the experimental data of Figure 8a. To optimize the simulations, phase difference (delays) between some components are required. The best β values are -0.5 unit of the external parameter for both the 1670- and 1637-cm^{-1} components and $\beta=0$ for all other components. Small differences can be observed in the intensities and shapes of some peaks of the experimental and simulated asynchronous maps, while many of the features are well reproduced. Therefore, like for GluRS, it seems that the loss of intramolecular β-sheets is delayed with respect to the formation of intermolecular β-sheets whereas the loss of α-helices is concomitant. Thus, apart from the presence of the small component due to turns at 1670 cm^{-1} that is also delayed, the aggregation mechanisms of GluRS and $G_{254}R$ involve the same secondary structures and the sequence of events are very similar, which suggests very close aggregation mechanisms, although the asynchronous maps are different.

CONCLUSION

2D-COS is based on the analysis of intensity variations occurring at independent wavenumbers. However, when a perturbation is applied, the spectral variations are rarely only due to intensity changes. Bandwidth changes and band shifts due to modification of the environment or physical state of the molecules are most often associated with intensity variations, especially when the perturbation is temperature. As a result, the features observed in 2D maps arise from the complex superposition of numerous parameters such as frequency shifts, changes in bandwidth, the band shape, and potentials delays or differences in the variation rates. Therefore, 2D maps are often too complex to be interpreted in a straightforward manner or it is impossible to discriminate whether 2D peaks originate from true asynchronisms or from other effects. This problem is more crucial for broad bands that are composed of several components. To overcome this problem, interpretation of 2D maps should be associated to other information or to simulations to be sure that asynchronous peaks are actually due to asynchronisms and not to spectral effects. In the present study, we have used curve-fitting and simulations, an approach that relies on some assumptions, especially regarding the fact that the waveform is chosen a priori. This type of approach might be considered as a step backward with respect to the conventional use of 2D-COS, which is a model-free method, but it is clearly necessary.

Although the present method is efficient in taking into consideration the shifts and bandwidth changes of the experimental data, it first suffers from the drawback of the multiplicity of the solutions given by curve-fitting. Different fits may lead to satisfying results and it is not sure that the optimal solution has been found. However, the results that have been presented are the best that have been obtained among many different attempts. Furthermore, as indicated above, the use of difference (dynamic) spectra strongly restricts the variations in the possible fits. In addition, it appears in practice that an even more restricted number of fits can give a good description of the experimental maps. Second, the choice of the waveform can be viewed as arbitrary. In fact, the aggregation of GluRS and Gr254 (mutant of GluRS) follows a sigmoidal form as seen from the evolution of the component at 1616 cm^{-1} (data not shown); thus the hyperbolic tangent function is a good representation of the process. Some attempts have been performed to observe the impact of the chosen waveform by modifying it drastically. For example, changing the hyperbolic tangent for an exponential does not have a strong impact on the asynchronous map of GluRS. More important are the delays between the components and the spectral effects. It is expected that the waveform influences the results, but in the present case this influence seems to be negligible with respect to other effects. We finally have to underline that the present method only works for parameter variations that are monotonic.

As a conclusion, since 2D maps can be too complex to be interpreted in a straightforward manner, there is a need for the development of methods that take the spectral effects into account. This goal reached, the 2D-COS method can be very powerful to provide very detailed information about the studied process, including the sequence of events and the possibility of band assignments. In this respect, additional efforts in the cautious application of 2D-COS to the analysis of the amide modes of proteins should provide significant insights into the complex denaturation–aggregation mechanism.

This work was supported by the Natural Science and Engineering Research Council (NSERC) of Canada, by the Fonds Québécois de la Recherche sur la Nature et les Technologies (FQRNT), and by the Centre de Recherche en Sciences et Ingénierie des Macromolécules (CERSIM). We thank Jacques Lapointe and Daniel Dubois (Département de biochimie, Université Laval) for purifying and providing us the wild-type and the mutant proteins and for several helpful discussions.

REFERENCES

1. Byler, D. M; Susi, H. Biopolymers 1986, 25, 469–488.
2. Surewicz, W. K.; Mantsch, H. H. Biochim Biophys Acta 1988, 952, 115–130.
3. Goormaghtigh, E.; Cabiaux, V.; Ruysschaert, J.-M. In Subcellular Biochemistry—Physicochemical Methods in the Study of Biomembranes; Hilderson, H. J., Ralston, G. B., Eds.; Plenum Press: New York, 1994; Vol 23, pp 405–450.
4. Krimm, S.; Bandekar, J. Adv Protein Chem 1986, 38, 181–364.
5. Kaupinen, J. K.; Moffatt, D.; Mantsch, H. H.; Cameron, D. G. Appl Spectrosc 1981, 35, 271–276.
6. Casal, H. L.; Köhler, U.; Mantsch, H. H. Biochim Biophys Acta 1988, 957, 11–20.
7. Noda, I. Bull Am Phys Soc 1986, 31, 520.
8. Noda, I. Appl Spectrosc 1990, 44, 550–561.
9. Noda, I. Appl Spectrosc 1993, 47, 1329–1336.
10. Nabet, A.; Pézolet, M. Appl Spectrosc 1997, 51, 466–469.
11. Meskers, S.; Ruysschaert, J.-M.; Goormaghtigh, E. J Am Chem Soc 1999, 121, 5115–5122.
12. Ozaki, Y.; Liu, Y.; Noda, I. Appl Spectrosc 1997, 51, 526–535.
13. Sefara, N. L.; Magtoto, N. P.; Richardson, H. H. Appl Spectrosc 1997, 51, 536–540.
14. Schultz, C. P.; Fabian, H.; Mantsch, H. H. Biospectroscopy 1998, 4, S19–S29.
15. Schultz, C. P.; Barzû, O.; Mantsch, H. H. Appl Spectrosc 2000, 54, 931–938.
16. Wang, Y.; Murayama, K.; Myojo, Y.; Tsenkova, R.; Hayashi, N.; Ozaki, Y. J Phys Chem B 1998, 102, 6655–6662.
17. Filosa, A.; Wang, Y.; Ismail, A. A.; English, A. M. Biochemistry 2001, 40, 8256–8263.
18. Paquet, M.-J.; Laviolette, M.; Pézolet, M.; Auger, Biophys J 2001, 81, 305–312.
19. Smeller, L.; Heremans, K. Vibr Spectrosc 1999, 19, 375–378.
20. Murayama, K.; Wu, Y.; Czarnik-Matusewicz, B.; Ozaki, Y. J Phys Chem B 2001, 105, 4763–4769.
21. Gericke, A.; Gadaleta, S. J.; Brauner, J. W.; Mendelsohn, R. Biospectroscopy 1996, 2, 341–351.
22. Czarnecki, M. A. Appl Spectrosc 1998, 52, 1583–1590.
23. Czarnecki, M. A. Appl Spectrosc 2000, 54, 986–993.
24. Söll, D.; Schimmel, P. R. In The Enzymes; Boyer, P. D., ed.; Academic Press: New York, 1974; Vol 10, pp 489–538.
25. Schimmel, P. R.; Söll, D. Ann Rev Biochem 1979, 8, 601–648.
26. Breton, R.; Sanfaçon, H.; Payannopoulos, I.; Biemann, K.; Lapointe, J. J Biol Chem 1986, 261, 10610–10617.
27. To be published.
28. Šašić, S.; Muszynski, Ozaki, Y. Appl Spectrosc 2001, 55, 343–349.
29. Noda, I. Appl Spectrosc 2000, 54, 994–998.
30. Carrier, D.; Mantsch, H. H.; Wong, P. T. T. Biopolymers 1990, 29, 837–844.
31. Pretrelski, S. J.; Tedeschi, N.; Arakawa, T.; Carpenter, J. F. Biophys J 1993, 65, 661–671.
32. Green, R. J.; Hopkinson, I.; Jones, R. A. L. Langmuir 1999, 15, 5102–5511.
33. Lefèvre, T.; Subirade, M. Biopolymers 2000, 54, 578–586.
34. Susi, H.; Timasheff, S. N.; Stevens, L. J Biol Chem 1967, 242(23), 5467–5473.
35. Clark, A. H.; Saunderson, D. H. P.; Suggett, A. Int J Peptide Protein Res 1981, 17, 353–364.